Available online at www.sciencedirect.com
ScienceDirect
Polymer Testing 25 (2006) 797–806
POLYMER TESTING
www.elsevier.com/locate/polytest

Property Modelling

Numerical and experimental studies of damage generation in a polymer composite material at high strain rates

A. Tasdemirci[a,b], I.W. Hall[a,*]

[a]Department of Mechanical Engineering, University of Delaware, Newark, DE 19716, USA
[b]Mechanical Engineering Department, Izmir Institute of Technology, Gulbahce 35437 Koyu, Urla, Izmir, Turkey

Received 19 March 2006; accepted 22 April 2006

Abstract

Samples of S2-glass/epoxy composites have been subjected to microstructural investigation after testing in compression at quasi-static and high strain rates using the split Hopkinson pressure bar. A numerical model was developed that accurately describes the high strain rate mechanical response of the samples. Moreover, in contrast with earlier phenomenological or constitutive models, the model can also predict a variety of failure modes such as delamination, matrix cracking or fiber crushing. High-speed photography was used to check the model results. Interrupted tests, followed by metallographic examination, have revealed that the sequence of damage events differs between quasi-static and high strain rate regimes. The effect of sample size on measured mechanical properties is noted and is confirmed via numerical modeling.

Keywords: S2-glass; Numerical simulation; LS-DYNA; Mechanical properties; High strain rate; Stress wave propagation

1. Introduction

A variety of studies have addressed failure modeling of composite materials under impact loading, e.g., [1–6]. Some of these have used the split Hopkinson pressure bar (SHPB) to study the dynamic properties of composites under compressive, tensile and shear loading conditions while others have used other techniques such as drop weight testing. Research efforts utilizing various versions of the SHPB to characterize dynamic properties of composites at high strain rates have mainly been focused on specimen geometry effects, through thickness stitching effects, fiber orientation effects, and strain rate effects. The present work focused instead upon using the SHPB as a means to validate a numerical model as well as generating reliable mechanical property data and investigating specimen size effects.

Song et al. [7] compared the quasi-static and high strain rate properties of an S2-glass/SC-15 composite as a function of orientation in a recent study and found the strain rate sensitivity to be more pronounced in the through thickness direction than the in-plane direction. They also presented a constitutive model that satisfactorily described the mechanical response of this composite in both testing directions and as a function of strain rate

*Corresponding author. Tel.: +1 302 831 1295; fax: +1 302 831 3619.
E-mail address: hall@me.udel.edu (I.W. Hall).

0142-9418/$ - see front matter © 2006 Elsevier Ltd. All rights reserved.
doi:10.1016/j.polymertesting.2006.04.011

although, in common with other currently used models, it was not able to account specifically for different fracture modes. Indeed, few experimentally supported studies have been reported concerning the fractographic details of the sequence of events involved in progressive failure in composites during Hopkinson pressure bar testing. In this paper, in addition to making such observations with the aid of interrupted tests, a rate-dependent progressive failure model was developed to account for the nonlinear and rate-dependent behavior commonly observed for fiber reinforced composite materials under high strain rate conditions and to investigate the sequence of deformation and fracture events leading to ultimate failure.

2. Experiments and modeling

S2-glass fiber woven fabric ($0.81\,kg/m^2$)/SC-15 epoxy (toughened resin) composite plates, 11.3 mm in thickness, were produced using the vacuum assisted resin transfer molding process. Cylindrical composite samples 11.0 mm in diameter were core-drilled from the plate in the through-thickness direction and samples were compression tested (a) quasi-statically at $1.1 \times 10^{-1}\,s^{-1}$ and (b) at various nominal strain rates between 595 and $1500\,s^{-1}$ using the SHPB. All tests were conducted with the compression axis normal to fiber plane. The particular SHPB apparatus used consists of Inconel 718 bars, a 356 mm long striker bar, 3450 mm incident and 1850 mm transmitter bars, all with a diameter of 19.05 mm. Multiple loading of the sample in SHPB was avoided by use of a transmitter bar shorter than the incident bar: this is crucial for identification of the microstructural damage progression during the loading period.

Briefly, in an SHPB test the striker bar generates a compressive elastic wave in the incident bar; this wave travels to the end of the bar where a portion of it enters the specimen and the rest is reflected back as a tensile wave. Of the portion of the wave entering the sample, some is reflected back at the sample/transmitter bar interface and the rest enters the transmitter bar, still as a compressive wave. Strain gages on the incident and transmitter bars record the passage of the wave and the data presented below are generally shown in this form, i.e. as the tensile or compressive waveforms recorded after the initial wave has interacted with the sample. The strain gage data were used for conventional data reduction using the 3-wave method and a dispersion correction was applied for all the data sets. Further details of the specific experimental set-up [8] and SHPB testing in general [9,10] are available elsewhere.

Several interrupted quasi-static and high strain rate compression tests were also conducted to allow evaluation of deformed microstructures as a function of increasing strain: a series of maraging steel collars were used to limit the maximum strain during the SHPB tests. Following testing, interrupted and fully loaded test samples were longitudinally sectioned and examined by optical and scanning electron microscopy. To study damage evolution in the samples in real time, a high-speed Ultra 8 camera was used to record the SHPB tests. The progression of damage was observed by photographing the specimen at predetermined intervals of the order of a few microseconds. With this high-speed camera, a maximum of eight frames could be recorded with an inter-frame time that could be varied between 10 ns and 1 ms.

The commercial explicit finite element code LS-DYNA 970 was used for three-dimensional SHPB finite element modeling. Numerical simulations were also carried out using a newly developed damage model, namely MAT 162, which has recently been incorporated into LS-DYNA. This model uses damage mechanics principles for progressive damage and material degradation. In the damage analysis of a composite specimen, a full-symmetric numerical model was used with appropriate boundary conditions. The model has three components in contact; the incident and transmitter bars each of length 1524 mm, and the specimen. A rectangular stress pulse is taken as the input to the impact face of the incident bar and all other boundaries are traction free and can move in any direction. In order to reduce computation time, the simulation uses bars 1524 mm in length instead of full-length bars and, although this decreases the transit time between successive waves and shortens the wave duration slightly, it does not affect the basic wave-shapes or amplitudes. Trial computations were carried out using full-length bars but, apart from the slightly smaller time window, no significant differences were found and the shorter bars were used in all calculations henceforth. The mesh includes a total of 292 800 elements, 52 800 elements for the specimen and 120 000 elements for each of the incident and transmitter bars. The composite specimen was modeled with 44 layers of elements in the thickness direction. Eroding single

surface contact was defined between the bar ends and the composite specimen.

Early development and validation of the model have been previously reported [11–13], principally for elastic deformation in multi-layer materials, but the present report concerns the first application to damage and fracture in a composite material. Briefly, if the output of the SHPB simulation exactly matches the experimentally measured response then the model is accurately capturing the details of wave propagation and damage generation inside the sample. The model can then be used with confidence to determine local conditions at any point within the sample: this information can be used, for example, to investigate when and where delaminations occur, fracture initiation sites, local stress gradients and stress discontinuities. Fracture of composites is highly statistical in nature and depends on the local population of defects so it cannot be expected that the model will exactly reproduce the actual fracture behavior since even small defects can influence damage initiation. Nevertheless, it will be seen that the model accurately reproduces the general appearance of the fracture path as it is revealed by high-speed photography and *post mortem* fractographic analysis; it thus achieves the main thrust of the present simulations which is to understand when and where damage starts and to see how it propagates.

3. Results

3.1. Quasi-static testing

Samples tested quasi-statically showed a maximum stress of ~660 MPa and a strain to failure of ~13%. Fig. 1 shows the stress/strain record from a typical compression test. The graph is essentially linear to >10% strain and shows a slight deviation from linearity just before final failure. Materialographic observations were made on samples tested either to varying degrees of strain or to complete failure, and the first signs of damage were not seen on the surface until almost 8% strain. Fig. 2(a) shows a polished and dye-infiltrated cross-section from a test interrupted at 8% strain showing that damage was limited to close to the outer surface. Microscopy at higher magnification confirmed that the damage was due to fine-scale delamination and was only detectable at >7% strain. Ultimate failure was preceded by severe delamination and the squeezing out sideways (hereafter termed 'extrusion') of segments of the woven layers, before complete failure occurred by shear along planes inclined at ~15° to the ply plane, Fig. 2(b). Matrix cracking was not observed until the very latest stages of fracture, typically >10% strain, and occurred mainly in association with regions that were extruded outwards.

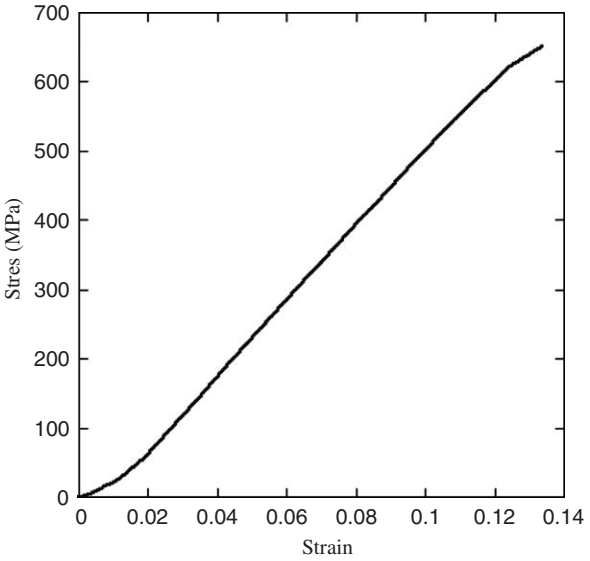

Fig. 1. Quasi-static stress–strain curves for S2-Glass/SC15 composite.

3.2. High strain rate testing

When compression testing with the SHPB, increasing the striker bar velocity leads to increasing strains as well as increasing strain rates but, for any given striker bar length, there is a minimum striker bar velocity which will cause failure for any given striker bar. This is illustrated in Figs. 3(a) and (b) which show typical sets of reflected and transmitted signals from SHPB experiments at average strain-rates in the range of 595–1500 s^{-1}. The experimental data have been grouped into (a) lower strain rate tests showing essentially elastic response with little damage and (b) higher strain rate tests showing the cumulative effects of damage on the reflected and transmitted signal shapes.

The dynamic compressive stress–strain curves show a nearly linear behavior at small strains (<2%) and then become nonlinear as the strain increases, Fig. 4. The initial portions of the stress–strain curves indicate that the composite is linearly elastic, without any damage at small strains.

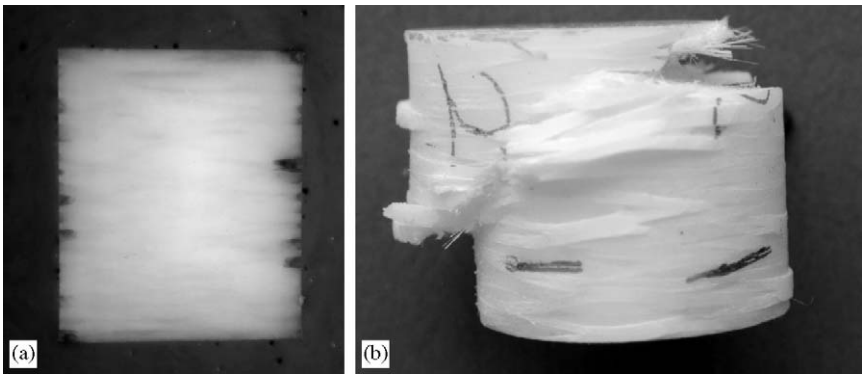

Fig. 2. Cross-sectional views of: (a) a test interrupted at 8% strain, (b) a sample loaded to complete failure.

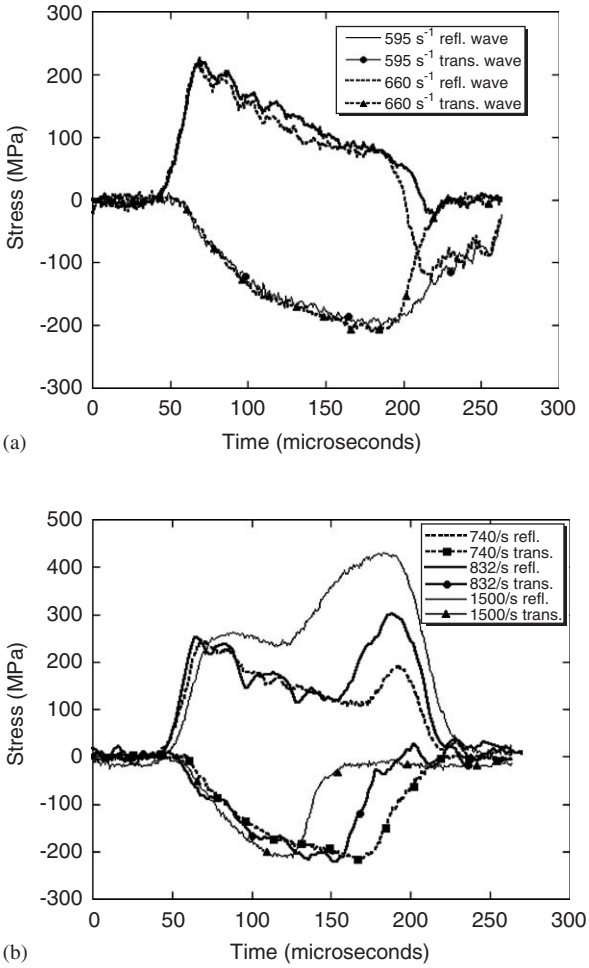

Fig. 3. Experimental bar output from strain gages on the incident and transmitter bars of composite specimens tested at various strain rates, (a) $\dot{\varepsilon} < 700\,s^{-1}$, and (b) $\dot{\varepsilon} > 700\,s^{-1}$.

The behavior becomes nonlinear at larger strains, indicating stress-induced damage and its accumulation with increasing strain, as reflected by the decreasing slope of the stress–strain curves. Furthermore, the compressive stresses at some fixed strain are slightly, but nonlinearly, sensitive to strain rate in dynamic groups. Except for those tested at strain rates less than $675\,s^{-1}$, the specimens failed completely during experiments. Fig. 4 also shows that the maximum engineering strain and stress before failure of the composite specimen along the through-thickness direction are approximately 10% and 700 MPa, respectively.

Fig. 5 shows, superimposed upon a typical stress vs. strain curve, photographs of samples compressed to various strains at the same strain rate of $800\,s^{-1}$. For low strain values, i.e., less than 2%, no visible damage was detected on the lateral surface of the specimen and stress–strain curves showed a nearly linear behavior. After 4% strain, damage occurred in some of the plies, appearing as discoloration/whitening at the fiber–matrix interfaces: this eventually resulted in some delamination, and was reflected by the decreasing slope of the stress–strain curve. Such delamination caused the transverse fibers to be extruded from the lateral surface of the specimen. Extensive cracking occurred at interlaminar boundaries, resulting in adjoining layers being displaced and extruded in different directions. At higher strains, and stress levels, catastrophic disintegration of the specimen was observed and the stress/strain curve suddenly dropped once the stress reached its maximum value.

High-speed photographs confirmed that damage could be visually observed well before the stress in the sample neared the peak value. Fig. 6 shows high-speed photographs of a test conducted at $809\,s^{-1}$ and shows clear experimental evidence of how damage occurred and propagated in the specimen. The frames were taken at 28 μs intervals,

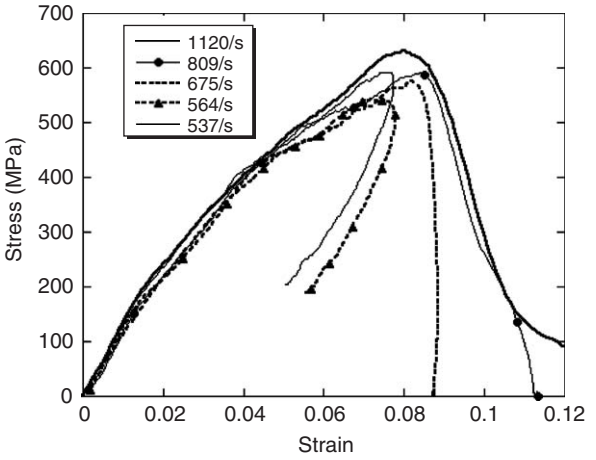

Fig. 4. Compression stress–strain curves of the composite in through thickness direction at different strain rates.

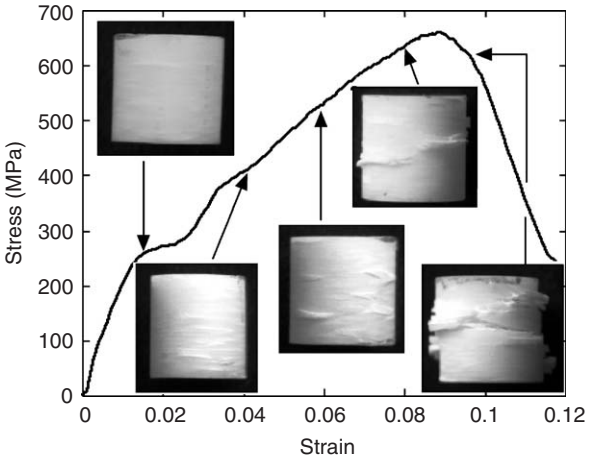

Fig. 5. Photographs of the specimens tested in the through thickness direction to various strains.

and each corresponds to an approximate 2% increase in strain. The first evidence of damage appeared at ~3% strain and always occurred close to the specimen/transmitter bar interface, at about three quarters of the specimen length. Thereafter, damage remained concentrated close to this region and final separation occurred on a plane inclined at a small angle (0–5°) relative to the plane of the plies.

Fig. 7 shows a recovered specimen after the test. Extensive cracking has occurred at interlaminar boundaries, resulting in adjoining layers being displaced and extruded in different directions and giving rise to two major fragments and several smaller ones. Cracks initiate between the fiber layers and also progressive shear cracks were observed in the matrix.

Finally, it is believed that a significant local temperature rise occurred during impact since the fractured parts had a distinct smell of burned resin. Although no dynamic temperature measurements were attempted, the high-speed photographs also appear to show fumes coming from the specimen surface, suggesting that heat generated during deformation may make an important contribution to the failure mechanism.

3.3. Numerical simulations

Figs. 8(a) and (b) show experimental and numerical results, respectively for an SHPB experiment conducted with a striker bar velocity of 18.2 m/s, corresponding to a strain rate of 850 s^{-1}. Fig. 8(a) shows the experimental results of different specimens tested under identical test conditions and illustrates the high degree of repeatability for these experiments in the early stages of the test. The amplitude of the reflected wave is seen to increase as a function of time from zero to a local maximum before decreasing gradually: this is followed by a sharp rise indicating that the specimen has been extensively damaged or has failed. Up to midway through the gradual decrease in amplitude, all the specimens show similar behavior. However, when disintegration begins, different unloading behaviors are observed because of the highly statistical nature of fracture as mentioned above. It is seen, however, that the numerical data of Fig. 8(b) show very similar behavior to the experimental data and, hence, confirm the validity of the model.

Fig. 9 shows details of the numerical model in which the contours for delamination damage were selected for plotting. The figure shows two views of the sample at three time increments. Close examination of the simulation shows compressive failure in the form of severe delamination concentrated in the region adjacent to the transmission face of the specimen, matching excellently with the actually observed damage modes. The longitudinal compressive strain generated lateral strains which promoted the development of interlaminar matrix cracks. Fiber bundles flowed outward from the specimen and eventually the specimen disintegrated catastrophically. Other damage contours were plotted showing the contribution and extent of matrix cracking and fiber breakage. It is seen that the model quite accurately reproduced the final appear-

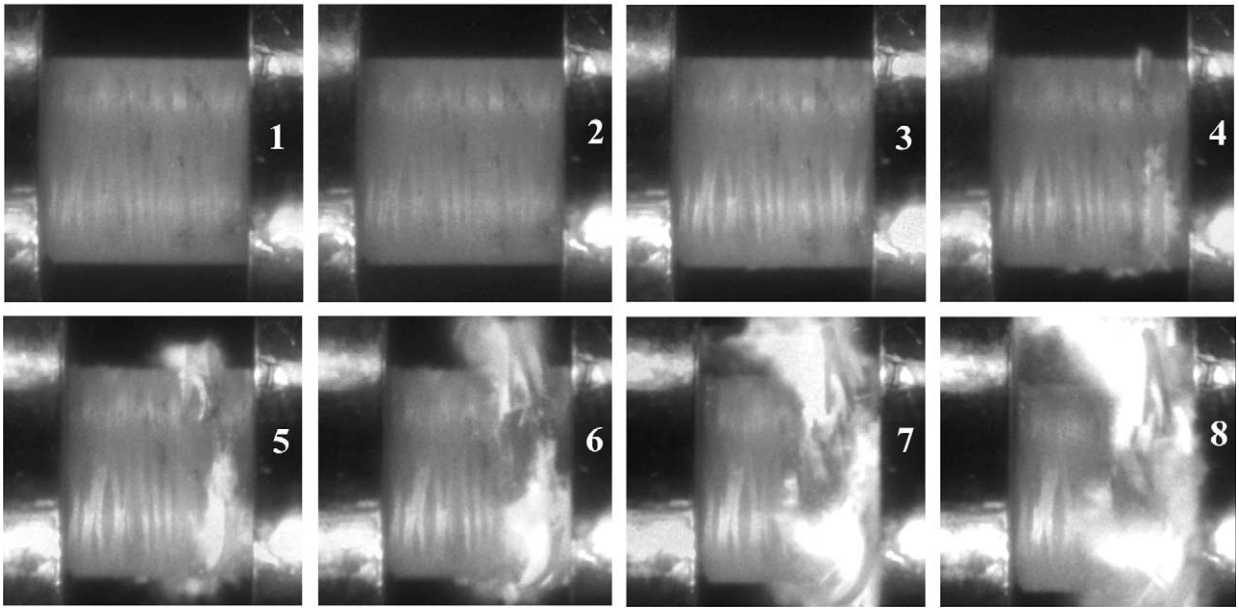

Fig. 6. High-speed photograph of real-time deformation of a composite specimen tested at an average strain rate of 809 s^{-1}. Interframe time 28 μs, exposure time 2 μs.

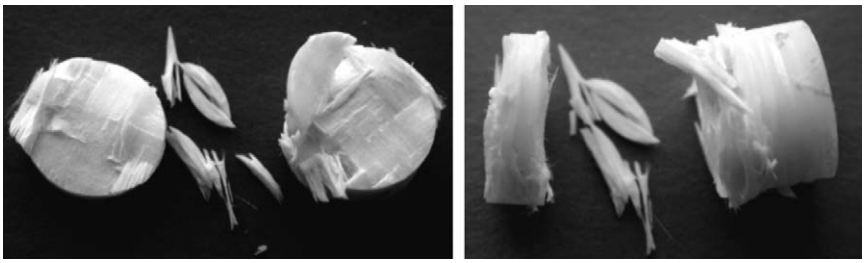

Fig. 7. Top and side views of the composite sample after testing at 18.2 m/s.

ance of fractured samples, see Fig. 7. For example, the final fracture plane was located close to the sample/transmitter bar interface and was almost normal to the compression axis.

4. Discussion

When comparing the results of the present work with those of prior investigations, several points of overlap and of difference emerge and it is instructive to consider these further. Perhaps the most closely similar recent investigation is that by Song et al. [7] who also tested S2 glass/SC-15 composites.

While both investigations reveal similar strengths for the composite, their measured strains to failure were significantly different, namely 10% and 7.5% under quasi-static and dynamic conditions, respectively [7] while the present work gave corresponding values of 13% and 10% i.e., considerably greater, and part of the reason for this may be found in the sample dimensions. Although of very similar diameter, the present samples had an aspect ratio h/d of ~1 while those of Song et al. [7] had an aspect ratio of 0.5. Since the matrix is strain rate sensitive, its yield stress increases during dynamic testing and makes it more likely that a competing deformation mechanism, such as delamination, will occur. Taller samples present (i) more locations for delamination and (ii) less interfacial constraint and, thus, produce higher strains to failure. This highlights the necessity of sample standardization for meaningful comparison of results.

Numerical calculations using samples with h/d of 0.5 and 1, confirm that the differences in measured

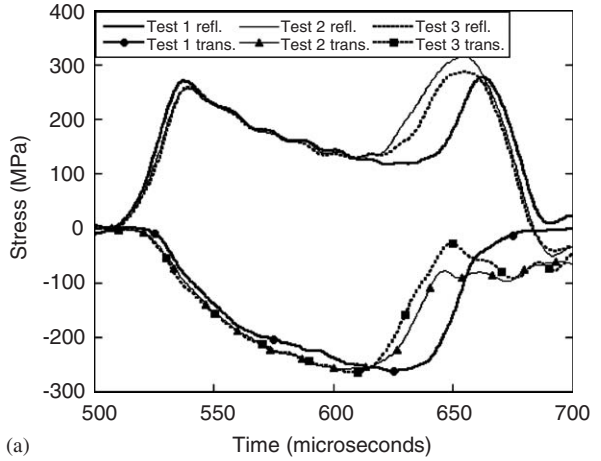

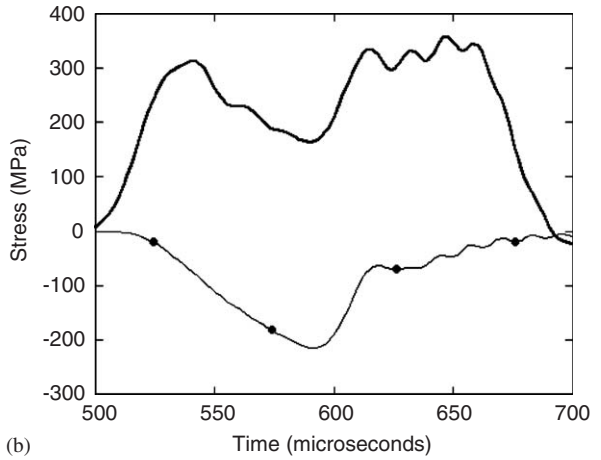

Fig. 8. (a) Experimental and (b) calculated output from strain gages on the incident and transmitter bars during a test on a composite sample.

properties and failure mode are related to the aspect ratio. The sample diameters were held constant at 11.00 mm. Fig. 10 shows a comparison of the calculated transmitted and reflected waves for both aspect ratio samples and significant differences are observed. Similarly, Fig. 11 presents a comparison of the fracture fragments at the same point in the test and different fragment sizes and shapes are observed.

A further notable feature of the present results is the almost complete absence of matrix cracking as a precursor to delamination. Stout et al. [14] studied C/epoxy laminate samples tested quasi-statically and identified matrix microcracking

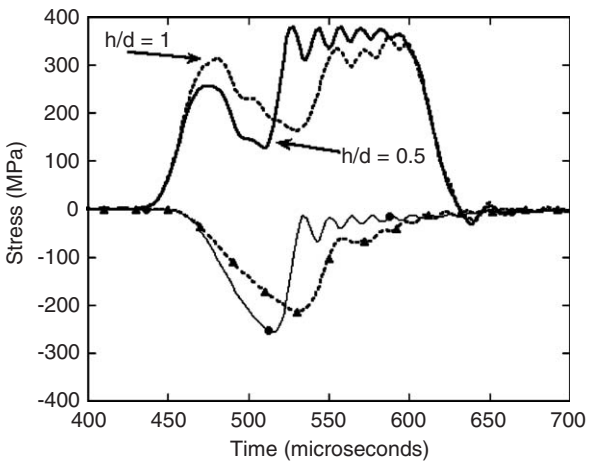

Fig. 10. Calculated output from strain gages on the incident and transmitter bars during a test on a composite sample for two different h/d ratios.

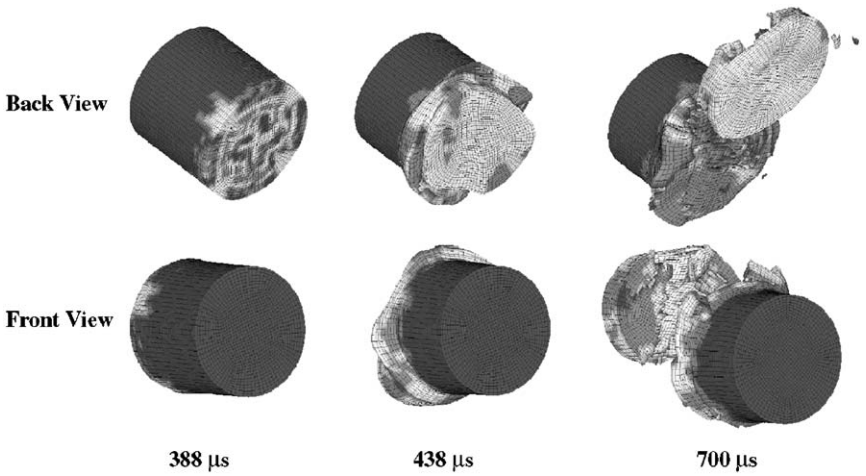

Fig. 9. Contours of progressive delamination damage.

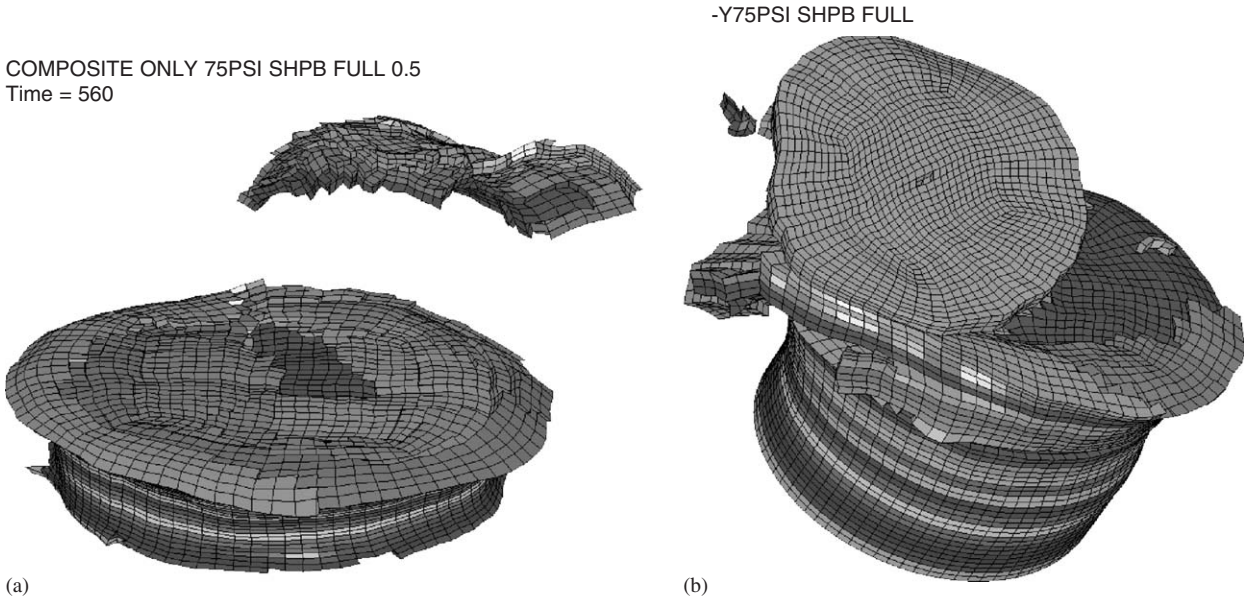

Fig. 11. Comparison of the fracture fragments of a composite specimen for two different h/d ratios: (a) 0.5 and (b) 1.0.

as a precursor to delamination in those regions of 4-point bend samples believed to experience only compressive loading. Matrix microcracking was also found to be the major cause of beam stiffness reduction. Other samples were tested dynamically in unsupported 2-point loading and again, although damage was confined to the rear two plies, matrix cracking was seen to precede delamination [14]. The absence of matrix cracking in the present samples strongly implies that matrix cracking is either not encountered under conditions of pure compression, leading to the conclusion that Stout et al's samples did indeed experience bending, or that its appearance is a function of the respective mechanical properties of the matrix and fiber combination.

Comparison of Figs. 2(a) and 5 show that the dynamically tested samples undergo more damage than quasi-statically tested samples as a function of strain and that, consequently, they are unable to maintain sufficient integrity to yield maximum loads and strains to failure equal to their quasi-statically tested counterparts. Stout et al. [14] also noted that more damage was induced at higher strain rates. The earlier onset of damage is reflected in the very different overall shapes of the stress vs. strain records. Quasi-static records are almost linear to failure (see Fig. 1) while dynamic ones show an early linear region, corresponding to purely elastic deformation, followed by a second approximately linear region after the onset of damage. Since the damage is not associated with matrix microcracking, the apparent reduction in modulus must be due to the onset of delamination and extrusion of the small segments as noted in Fig. 5.

In view of the rather irregular appearance of the high strain rate stress vs. strain graphs, some tests were repeated with copper disk pulse-shapers. While these experiments produced smoother graphs and less variation in strain rate throughout the test, the large-scale irregularities could not be eliminated. Similar experiments by Gama [15] using identical material with an h/d ratio of approximately 0.5, showed the same type of irregularities. In contrast, Song et al. [7] presented smooth graphs for their material with an h/d ratio of 0.5, although they used the one-wave method of data reduction rather than the three-wave method used in the present work [9,10]. In order to investigate this aspect, the model was interrogated to derive the stress vs. strain graphs corresponding to the 1-wave and 3-wave data-reduction procedures and it is concluded that these irregularities reflect actual processes occurring within the composite and are not artifacts of the data-handling procedure.

Once again, the importance of sample dimensions becomes evident since the observed reduction is most likely a consequence of edge effects and would be minimized in larger samples; unfortunately, testing of larger samples is beyond the capabilities

of our present apparatus. The samples of Song et al. [7] showed a much more gradual reduction in the slope of the stress/strain curves at high strain rate, an effect possibly, again, linked to the sample size since their samples were only half the height of the present ones and, hence, much less susceptible to edge effects. Also, it has been shown that the dynamic response of E-glass/epoxy composites is strongly influenced by thickness [6].

A major contribution of this work, however, has been to demonstrate the development and validation of a numerical model to accurately describe the progression of deformation and damage in the composite plates: further refinement of the model is underway. Recent researchers [7] defined a scalar damage parameter to characterize the degree of damage accumulation in the specimen during the deformation. This approach cannot distinguish the individual failure modes and their effects on the mechanical properties whereas the numerical material model used here can handle and easily distinguish different failure modes. Furthermore, the previous composite failure model adopted within LS-DYNA was a 2D failure model, and the failure mode due to out-of plane shear and normal stresses were neglected. While this may be sufficient for composite structures under in-plane loading, this model may be unable to capture transverse impact failures for which all six stress components are known to contribute to damage development. The numerical material model used presently, however, is based on the 3D stress field and can be used to effectively simulate fiber failure, matrix damage, and delamination behavior under all conditions—opening, closure, and sliding of failure surfaces. Furthermore, this progressive failure modeling approach is advantageous as it enables one to predict delamination when locations of delamination sites cannot be anticipated; i.e., locations of potential delamination initiation are calculated without a priori definition of an interlaminar crack surface. Also, post failure modeling is improved relative to previous models by utilizing a damage mechanics approach to reduce mesh sensitivity. This failure model has been successfully utilized to characterize the impact damage in composite structures for a wide range of impact problems.

Reliable material models that accurately describe the responses of polymer-based composites under high strain rate loading conditions are vital for structural design and optimization studies. The study reported here verified that this newly implemented material model can successfully capture the fracture and deformation behavior of the composite investigated in this study.

5. Conclusions

A numerical model has been developed to investigate the compressive deformation and fracture of an S2-glass/epoxy composite. Excellent agreement has been demonstrated for the case of high strain rate loading and in all cases the region of final fracture was located just behind the sample/transmitter bar interface. Also, the fracture plane was successfully predicted to be at a small angle to that of the plies. The predicted mode and location of fracture were verified by high-speed photography.

Acknowledgments

The authors gratefully acknowledge financial support from the Army Research Office under Contract Number 47335-EG, Program Manager Dr. Bruce LaMattina, and the National Science Foundation under Grant INT-0242772, Program Manager Dr. O. Shinaishin.

References

[1] S. Abrate, Modeling of impact on composite structures, Compos. Struct. 51 (2001) 129–138.
[2] H.Y. Choi, F.K. Chang, A model for predicting damage in graphite epoxy laminated composites resulting from low-velocity point impact, J. Compos. Mater. 26 (14) (1992) 2134–2169.
[3] F. Collombet, et al., Damage criteria for the study of impacted composite laminates, Compos. Sci. Technol. 58 (5) (1998) 679–686.
[4] F. Collombet, X. Lalbin, J.L. Lataillade, Impact behavior of laminated composites: physical basis for finite element analysis, Compos. Sci. Technol. 58 (3–4) (1998) 463–478.
[5] G.A.O. Davies, X. Zhang, Impact damage prediction in carbon composite structures, Int. J. Impact Eng. 16 (1) (1995) 149–170.
[6] J.K. Kim, K.W. Kang, An analysis of impact force in plain-weave glass/epoxy composite plates subjected to transverse impact, Compos. Sci. Technol. 61 (1) (2001) 135–143.
[7] B. Song, W.N. Chen, T. Weerasooriya, Quasi-static and dynamic compressive behaviors of a S-2 glass/SC15 composite, J. Compos. Mater. 37 (19) (2003) 1723–1743.
[8] A. Tasdemirci, Experimental and modeling studies of stress wave propagation in multilayer composite materials, Ph.D. Dissertation in Mechanical Engineering. University of Delaware, Newark, 2005. p. 240.

[9] G.T. Gray III., High strain rate testing of materials: the split-Hopkinson pressure bar, in: Methods in Materials Research, Wiley, New York, 1997.
[10] G.T. Gray III., Classic split-Hopkinson pressure bar testing, in: H. Kuhn, D. Medlin (Eds.), ASM Handbook. Mechanical Testing and Evaluation,, ASM International: Materials Park, OH, 2000 pp. 462–476.
[11] A. Tasdemirci, I.W. Hall, Numerical and experimental studies of damage generation in multi-layer composite materials at high strain rates. International Journal of impact Engineering (2005), in press.
[12] A. Tasdemirci, I.W. Hall, Experimental and modeling studies of stress wave propagation in multilayer composite materials: low modulus interlayer effects, J. Compos. Mater. 39 (11) (2005) 981–1005.
[13] A. Tasdemirci, I.W. Hall, B.A. Gama, M. Guden, Stress wave propagation effects in two- and three-layered composite materials, J. Compos. Mater. 38 (12) (2004) 995–1009.
[14] M.G. Stout, et al., Damage development in carbon/epoxy laminates under quasi-static and dynamic loading, Compos. Sci. Technol. 59 (16) (1999) 2339–2350.
[15] B.A. Gama, Split Hopkinson pressure bar technique: experiments, analyses and applications, Ph.D. Dissertation in Material Science. University of Delaware, Newark, 2004. p. 385.